Journal of Oceanography, Vol. 66, pp. 349 to 361, 2010

Structure and Seasonal Variability of the Deep Mean Circulation of the East Sea (Sea of Japan)

YOUNG JIN CHOI[1]* and JONG-HWAN YOON[2]

[1]*Graduate School of Maritime Sciences, Kobe University, Fukaeminami-machi, Higashinada-ku, Kobe 658-0022, Japan*
[2]*Research Institute for Applied Mechanics, Kyushu University, Kasuga-koen, Kasuga, Fukuoka 816-0811, Japan*

(Received 1 October 2008; in revised form 22 January 2010; accepted 25 January 2010)

The horizontal structure of deep mean circulation and its seasonal variability in the Japan/East Sea (JES) were studied using profiling float and moored current meter data. The deep circulation in the Japan Basin (JB) flows cyclonically, basically following f/H contours. The correlation between the directions of deep current and f/H contour increases as $|\nabla(f/H)|$ increases, reaching remarkably high correlation coefficient (>0.8) values in steep slope regions in the JB. In contrast to the JB, the deep mean circulation in the Ulleung/Tsushima Basin (UTB) is generally weak and cyclonic accompanied by sub-basin-scale cyclonic and anticyclonic eddies. The UTB shows a poorer correlation between directions of deep current and f/H contours than other basins. The time-space averaged deep mean current is about 2.8 cm/s and the volume transport in the deep layer (800 m to bottom) in the JB reaches about 10 Sv (10×10^6 m^3s^{-1}), which is about four times greater than the inflow transport through the Tsushima Straits. A salient feature is that the amplitude of deep mean current in the JB reveals a remarkable seasonal variation with a maximum in March and minimum in October. The annual range of the seasonal variation is about 30% of the mean velocity, whereas that in the southern JES (UTB and Yamato Basin) is weak.

Keywords:
· Sea of Japan,
· deep mean current,
· seasonal variability,
· PALACE float,
· f/H,
· eddy-topography interaction,
· baroclinic instability.

1. Introduction

The Japan/East Sea[§] (JES) is a semi-enclosed marginal sea surrounded by Korea, Japan, and Russia. It connects with surrounding seas through very shallow, narrow straits: the Korea/Tsushima Straits connecting with the East China Sea, the Tsugaru Strait connecting with the Northwest Pacific and the Soya and Tatar straits connecting with the Okhotsk Sea. The average depth of the JES is about 1500 m, but the maximum depth of these three straits is less than 150 m. Therefore, the deep circulation in the JES is considered to be independent of that in the Northwest Pacific. The deep layer of the JES consists of three basins: the Japan Basin (JB), the Ulleung[¶]/Tsushima Basin (UTB), and the Yamato Basin (YB), with maximum depths of 3700, 2500, and 2900 m, respectively (Fig. 1).

Since the deep layer from 500 m to the bottom is occupied by the Japan Sea Proper Water (JSPW) with almost uniform density horizontally and vertically, the deep velocity cannot be obtained by standard dynamic calculation. Many efforts have therefore been made to measure the deep current directly, starting in the 1980s (e.g., Kitani, 1987). However, measurements have been conducted only in limited areas and for limited durations, until "the Cold War" ended in 1991. Since that time, the oceanic circulation of the JES has been investigated intensively in international cooperative studies, such as the Circulation Research of the East Asian Marginal Seas (CREAMS) (Danchenkov *et al.*, 2003). During the CREAMS (1993–1997) campaign, many direct current measurements were obtained in the deep layer in the JES, especially in the northern half of the JES, revealing that the currents in the layer below 1000 m depth are vertically coherent, accompanied by strong mesoscale activities with velocities occasionally exceeding 30 cm/s in the

* Corresponding author. E-mail: choiyj@port.kobe-u.ac.jp

§ The Editor-in-Chief does not recommend the usage of the term "East Sea", "East/Japan Sea", or "Japan/East Sea" in place of "Sea of Japan" or "Japan Sea".

¶ The Editor-in-Chief does not recommend the usage of the term "Ulleung Basin" in place of "Tsushima Basin".

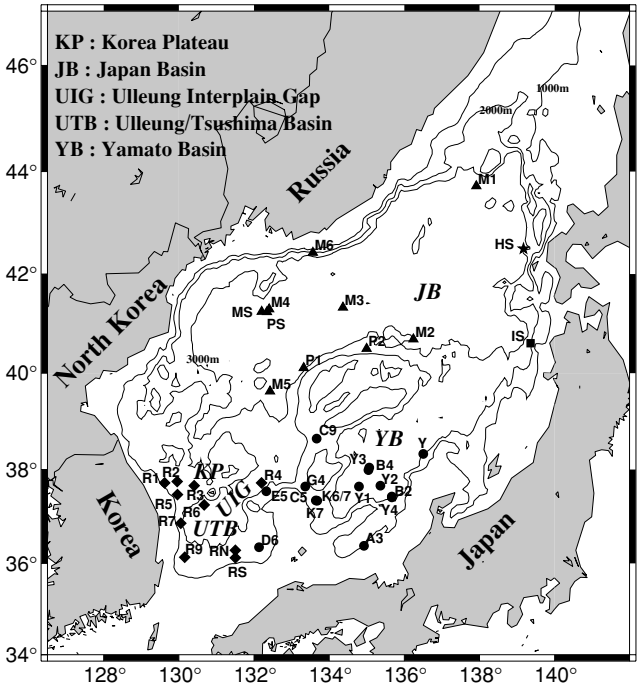

Fig. 1. Bathymetry and mooring stations in the JES. Triangles indicate Prof. Khromov's observation points, diamonds indicate observations of the University of Rhode Island, circles represent Kakuyo-maru observation sites, square represents mooring site of Oshoro-maru, and star is the observation point of Hokkaido Prefectural Central Fisheries Experiment Station, respectively. Note that we only have an annual average for the HS point. †The "Ulleung Interplain Gap" corresponds to the "Oki Gap". ¶The Editor-in-Chief does not recommend the usage of the term "Ulleung Basin" in place of "Tsushima Basin".

JB. These values were obtained from long-term moored current meter observations at seven mooring sites (Takematsu *et al*., 1999). Takematsu *et al*. (1999) also reported a strong seasonal variability of eddy-like deep currents, which have a tendency to intensify from late winter to early spring and weaken toward summer at a few mooring sites in the deep layer of the JB. However, due to the limited number of mooring sites and short durations of the measuring campaigns, the detailed structure of the deep circulation, e.g., horizontal distribution of velocity field and its seasonal variability has not yet been well clarified.

Senjyu *et al*. (2005) obtained mean current vectors at 69 sites in the JES deep layer using moored current meter data obtained from October 1986 to June 2003. The period for which current meters are moored at each site is mostly about 1 year or less. The results suggested a relatively strong cyclonic circulation in each basin along the basin periphery and weak currents in each basin interior. However, the number of mooring sites and the mooring duration at each site are still inadequate to detect the detailed structure of the deep circulation and its seasonal variability. Actually, the circulation in the UTB is not as simple as Senjyu *et al*. (2005) suggest.

Teague *et al*. (2005) used Pressure-gage-equipped Inverted Echo Sounder (PIES) observations (1999 to 2001) to reveal that the deep circulation in the UTB consists of at least two cyclonic cells. Additionally, according to Chang *et al*. (2002), the deep flow in the UTB involves a wide range of time scales with no apparent seasonal variations, unlike the findings of Takematsu *et al*. (1999).

The deep circulation at 800 dbar depth in the JB was also investigated using trajectories of Profiling Autonomous Lagrangian Circulation Explorer (PALACE) floats from 1999 to 2001 (Danchenkov *et al*., 2003), which suggest a large cyclonic gyre following roughly 3000 m isobaths in the JB, as Senjyu *et al*. (2005) suggested. Danchenkov *et al*. (2003) also revealed that the large cyclonic gyre in the JB is a recirculating cyclonic gyre with a diameter of 190 km at its largest and a center at (41.5°N, 133.5°E) in the eastern part of the gyre. The average speed of floats drifting around the recirculating gyre was about 2~3 cm/s with a maximum of up to 18 cm/s. However, due to the absence of a statistical analysis of profiling float trajectories, the detailed horizontal structure of the deep mean current as well as its seasonal variability has not yet been well clarified.

Thus, past current meter observations at a limited number of mooring sites and previous float analysis have not been able to clarify the detailed horizontal structure and the seasonal variability of the deep mean circulation of the JES in the JB and YB. In this study we investigate the detailed horizontal structure of mean velocity and volume transport in the deep layer in the JES, especially in the JB and YB, using profiling float trajectories obtained during a 7-year period from 1999 to 2006, covering most of the JES. The seasonal variability of the deep mean currents is also studied using both float trajectories and mooring data. As for the UTB, the structure of the deep mean circulation is studied in detail with a more accurate estimation of velocity than that reported in Park *et al*. (2004) using APEX float data from METRI (Meteorological Research Institute) from 2001 to 2006.

Section 2 contains a description of the observed data and its processing. Horizontal structures of the deep mean velocity field, the volume transport, and the seasonal variability of mean circulation in the JES deep layer are studied in Section 3. In Section 4, which comprises the summary and discussion, we propose a hypothesis concerning a possible mechanism of seasonal variability of the deep current.

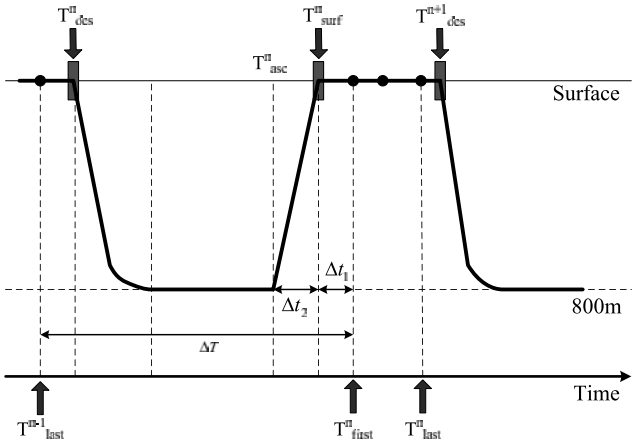

Fig. 2. Diagram of a float cycle. Dots on the surface indicate satellite fixes of the float at the sea surface. T^n_{des}(T^n_{asc}) is the time a float begins to descend(ascend) from the sea surface (parking depth), T^n_{first}(T^n_{last}) is the first(last) transmission position, respectively.

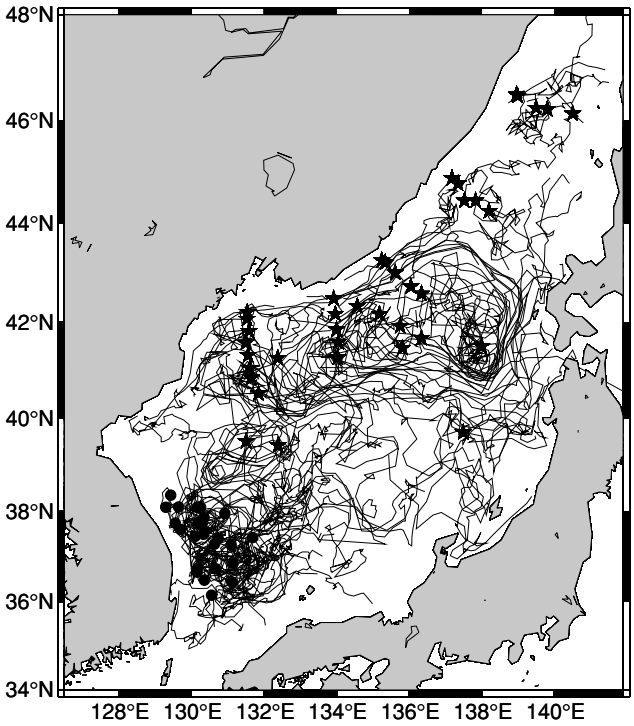

Fig. 3. Spaghetti plots of trajectories of 38 PALACE floats and 27 APEX floats drifting at 800 m depth in the JES. Stars indicate starting positions of PALACEs whereas circles indicate starting points of APEXs, respectively.

2. Data and Processing

2.1 Profiling floats

In total, 38 PALACE floats were deployed in the northern part of the JES during the Office of Naval Research (ONR) JES project (Danchenkov *et al*., 2003) in summer 1999 to study the surface and intermediate circulation. From 2001 to 2006, 27 APEX floats were deployed, mostly in the UTB, by METRI under the ARGO project. These floats were set to drift at around 800 dbar depth. The entire observation period of the PALACE floats ran from August 1999 until January 2004, and that of the APEX floats ran from December 2001 until September 2006. The residence times of PALACE floats ranged from 8 to 1643 days with a mean residence time of 527 days, while those of the APEX floats ranged from 56 to 1638 days with a mean residence time of 662 days. One cycle of each float was completed in about 7 days and 19 hours, during which approximately 7 days were spent parked at depth (800 dbar), about 2.5 hours rising to the surface, 12 hours at the surface, transmitting data to the ARGOS and getting surface fixes (positionings), and about 4.5 hours descending back to the parking depth. The float also recorded a vertical profile of temperature, salinity and depth during ascent. These operations were repeated from dozens of times to about 100 times. A diagram of a typical cycle is shown in Fig. 2.

The *n*-th cycle starts at T^n_{des} when a float begins to descend from the sea surface to its parking depth. As it surfaces at T^n_{surf}, it becomes ready to transmit data to an ARGOS satellite. Communication positions at the surface, indicated by dots, are the so-called "fixing position" or "fix". The float remains at the sea surface long enough to ensure that an ARGOS satellite receives the information. Data transmissions terminate with the beginning of the next, (*n*+1)-th cycle at T^{n+1}_{des}. Figure 3 shows the entire set of trajectories of the 38 PALACEs and the 27 APEXs, where stars and circles indicate release points of PALACEs and APEXs, respectively. The trajectories are dense in the JB and UTB, but sparse in the Yamato Basin and east of North Korea, suggesting that floats deployed in the JB (UTB) reside mostly within the JB (UTB), resulting in sparse trajectories east of North Korea and in the Yamato Basin.

Yanagimoto and Taira (2003) showed that the parking depths of the profiling floats in the JES tend to decrease as a result of mechanical problems such as leakage of the hydraulic oil or erosion of the bodies. We excluded 253 displacement velocities (about 5.8%) with parking depths shallower than 500 m.

The mean velocity at the parking depth during the cycle "*n*" of a float can be roughly estimated as

$$(U^n_{deep}, V^n_{deep}) = [(lon,lat)^n_{first} - (lon,lat)^{n-1}_{last}]/\Delta T, \quad (1)$$

where U^n_{deep} and V^n_{deep} are the mean drifting velocities at the parking depth for the cycle "*n*", (*lon*,*lat*) represents

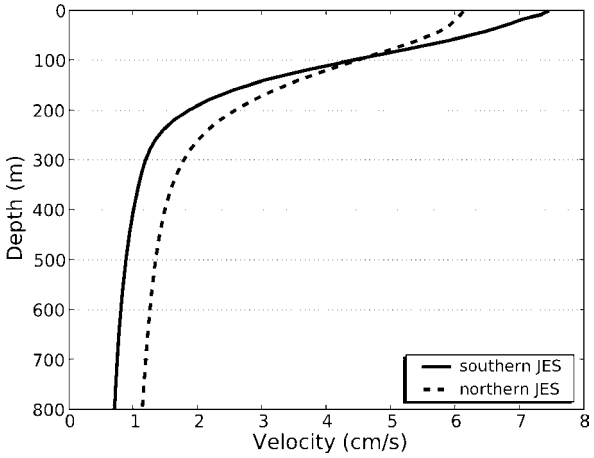

Fig. 4. Vertical velocity distributions from the surface to 800 m depth in the southern JES (south of 40°N, solid line) and the northern JES (north of 40°N, dashed line), respectively.

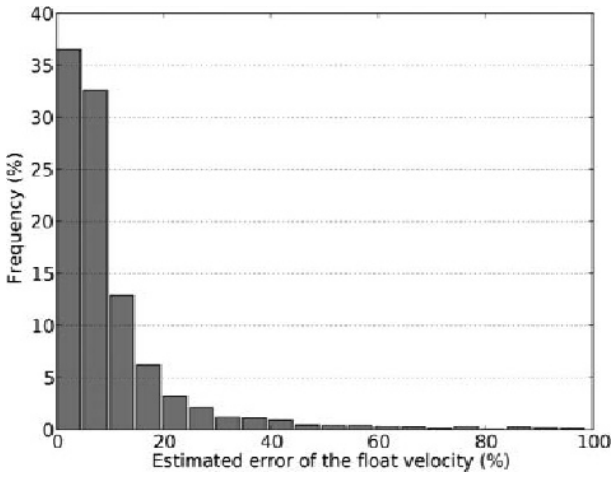

Fig. 5. Histogram of estimated error in drifting velocity amplitude at parking depth.

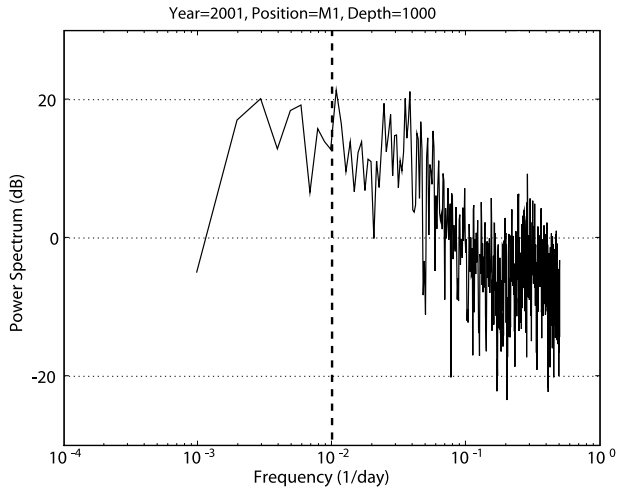

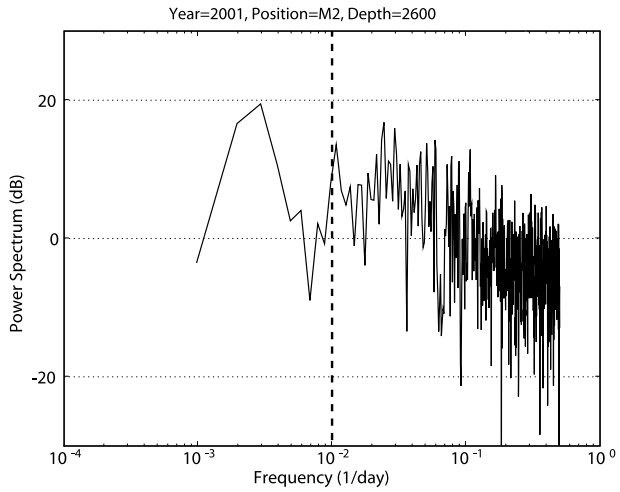

Fig. 6. Power spectral density of the current meter time series of M1 at 1000 m (upper) and M2 at 2600 m (lower), respectively. Dashed lines indicate 100 days frequency.

the position of fix, and ΔT represents the time interval between the first fix of the cycle "n", T^{n}_{first} and the last fix of a cycle "$n-1$", T^{n-1}_{last}, respectively. However, this simple estimation of the drifting velocity at the parking depth (800 dbar) contains errors originating from a) surface drift, b) drift during ascent and descent, and c) positioning error. To estimate these errors we rely on two assumptions: first, ocean currents flow in the same direction from the sea surface to 800 dbar depth. Secondly, assumption is that the positioning error is negligible because the positioning error is about 10 times smaller than the other errors. According to Ichikawa *et al*. (2001), the maximum value of the positioning error is 0.1 cm/s in the Kuroshio region. The error resulting from drift after surfacing, ε_1, can be estimated as:

$$\varepsilon_1 = V_s \Delta t_1 / \Delta T, \tag{2}$$

where V_s is a surface velocity calculated from the surface fix positions and times, Δt_1 is the time between surfacing and the first fix, which is assumed to be 0.91 hour according to Ichikawa *et al*. (2001). The error ε_2 caused by drifting during ascending and descending can be expressed as

$$\varepsilon_2 = (\Delta T)^{-1} \int_0^{\Delta t_2} V(z) dt, \tag{3}$$

where Δt_2 is the time taken to surface and $V(z)$ is a horizontal velocity at a level z.

Table 1. Summary of current meter data described in the text. Each column indicates: Observation ship name (Ship), mooring site (Site), latitude (Lat), longitude (Lon), current meter depth (Depth), and observation periods (from start time (Start) to end time (End)), respectively.

Ship	Site	Lat	Lon	Depth	Start	End
Khromov	M1	43.72	137.91	1000/2000/2500	Aug. 1993	Jun. 2001
	M2	40.69	136.24	1000/2000/2600	Aug. 1993	Jun. 2001
	M3	41.33	134.36	1000/2000/3000	Aug. 1993	Aug. 1996
	M4	41.30	132.40	1300/2100/2900	Jul. 1994	Aug. 1995
	M5	39.63	132.42	900/1900/2400	Jul. 1994	Aug. 1996
	M6	42.42	133.56	800/1800/2400	Aug. 1995	Jun. 2003
	MK	41.00	133.50	1000/3000	Jul. 2000	Jul. 2001
	MS	41.25	132.20	1700/2500/3200	May 1999	Jul. 2001
	P1	40.11	133.32	1000/3000	Aug. 2000	Jul. 2002
	P2	40.50	134.99	1000/2500	Aug. 2000	Jul. 2002
	PS	41.24	132.34	1000/2800	Jul. 2000	Jul. 2001
Kakuyo	A3	36.38	134.92	400/700/600	May 1995	May 1997
	B2	37.43	135.66	1000/2500	Jun. 1999	Jun. 2000
	B4	37.99	135.04	1000/2000	Jun. 1999	Jun. 2000
	C5	37.34	133.64	1000/1400	Jun. 1999	Jun. 2000
	C9	38.65	133.66	900/2000	Jun. 1998	Jun. 2000
	D6	36.35	132.13	1000/1400	Jun. 1998	Jun. 2001
	E5	38.33	136.5	1000/2000	Jun. 2002	Jun. 2003
	G4	37.54	132.32	1500	Jun. 2002	Jun. 2003
	K6	37.99	135.04	1000/2000	Jun. 2002	Jun. 2003
	K7	37.35	133.64	1000/1500	Jun. 2001	Jun. 2002
	Y	37.43	135.66	1000/2500	Jun. 2000	Jun. 2001
	Y1	37.64	134.79	800/1800/2800	Jun. 1997	Jun. 1998
	Y2	37.66	135.36	700/1800/2800	Jun. 1997	Jun. 1998
	Y3	38.04	135.06	800/1900/2800	Jun. 1997	Jun. 1998
	Y4	37.41	135.66	1700	Jun. 1998	Jun. 1999
Melville	R1	37.72	129.62	1200	Jun. 1999	Jun. 2001
	R2	37.75	129.95	1600	Jun. 1999	Apr. 2001
	R3	37.66	130.40	1600	Jun. 1999	Jul. 2001
	R4	37.72	132.20	2500	Jun. 1999	Jun. 2001
	R5	37.47	129.96	1500	Jun. 1999	Jul. 2001
	R6	37.24	130.67	2200	Jul. 1999	Jun. 2001
	R7	36.86	130.05	2200	Jun. 1999	Jul. 2001
	R9	36.13	130.15	1500	Jun. 1999	Jun. 2001
	RN	36.28	131.50	1800	Jun. 1999	Jun. 2001
	RS	36.12	131.50	1500	Jun. 1999	Jun. 2001
Oshoro	IS	40.61	139.36	300/2100	Apr. 1994	Apr. 1995

The initial descent of a float is relatively rapid and it takes less than 1 hour to reach half the target depth (Davis *et al*., 1992). The float then takes a larger time to arrive the parking depth. The $V(z)dz$ becomes very small around the equilibrium parking depth. Even though the descent times of floats are more than double the ascent times, this feature leads us to assume that both ascent and descent times are the same, following Ichikawa *et al*. (2001).

The total error of the current velocity at a parking depth can then be expressed as follows:

$$\varepsilon = \sqrt{2 \times (\varepsilon_1 + \varepsilon_2)^2}, \quad (4)$$

since ε_1 and ε_2 have the same sign, and errors will occur in both ascent and descent.

We estimate the error ε_2 using numerical model current data instead of geostrophic vertical shear, unlike Ichikawa *et al*. (2001). The model current data are supplied by the RIAM operational Japan Sea prediction system at Kyushu University (http://oops.riam.kyushu-

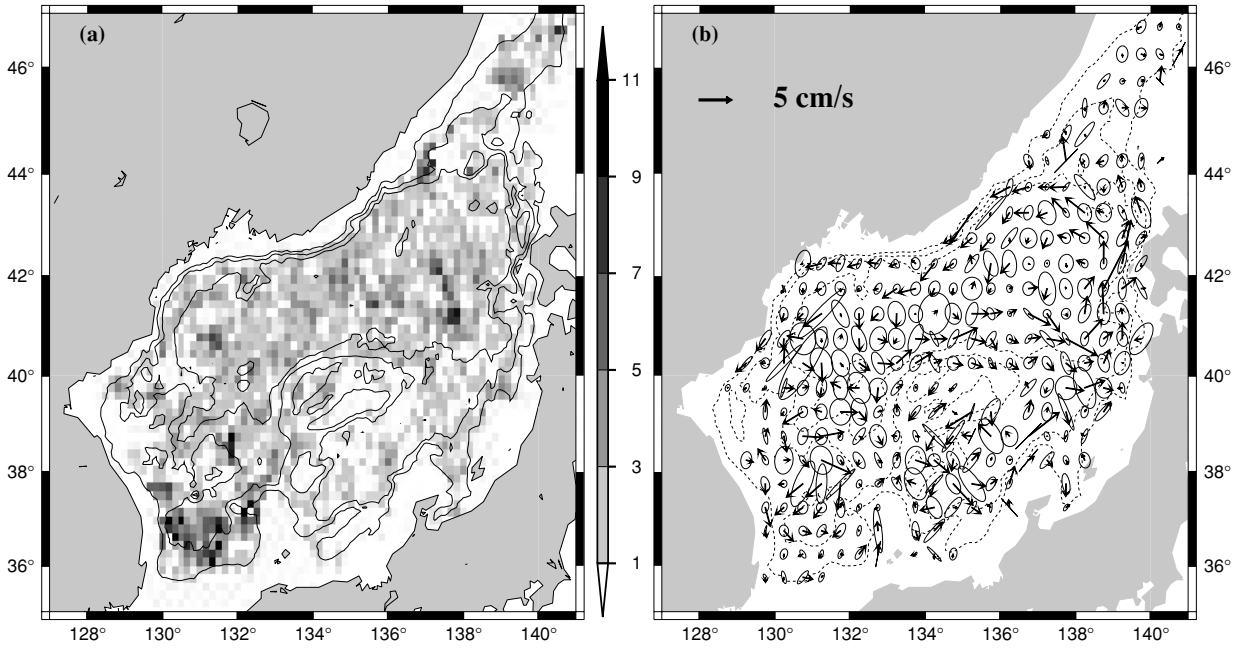

Fig. 7. (a) Number of velocity data from float trajectory per one grid (1/6°) and (b) weighted averaged velocities and standard error ellipses (with 90% confidence), which are centered on the origins of the velocity vectors, respectively. Error ellipses and mean velocities are sampled every 3 grids (1/2°) and contour lines (solid or dashed) of both panels indicate topography at the 1000 m interval.

u.ac.jp/vwp/, Hirose *et al*., 2007), with 1/12° horizontal resolution and 36 vertical levels. The climatological annual average of the model current data is calculated using daily forecast current data from January 1, 1998 to December 31, 2007. Considering the significant differences between circulation patterns in the northern and southern regions, two mean vertical profiles of model horizontal velocity are used as $V(z)$. One is obtained by averaging horizontal model velocity in the northern region (39°N~44°N, 130°E~139°E), and the other in the southern region of the JES (35°N~39°N, 129°E~139°E). These profiles are shown in Fig. 4.

Ichikawa *et al*. (2001) suggested that the total error ε in a drift velocity at a parking depth ranged from 10 to 25% in the Kuroshio region, and this has been widely accepted in other studies (Xie *et al*., 2005; Sallée *et al*., 2006; Tomczak, 2007). However, in this study the average of errors is about 0.14 cm/s, which corresponds to 5.0% of the mean velocity at a parking depth. The drift error in the JES is much smaller than in the Kuroshio region. Figure 5 shows a histogram that compares estimated errors with estimated velocities (error/velocity × 100%) at the parking depth from profiling floats.

2.2 Mooring current meter data

Many long-term direct current measurements were conducted in the deep basins in the JES using mooring systems between 1993 and 2003. The deep current data used in this study were collected by mooring systems deployed and recovered by the Russian R/V "Professor Khromov", "Kakuyo-maru" of Nagasaki University, "Oshoro-maru" of Hokkaido University, and R/V "Melville" under a joint program between the University of Rhode Island and the Naval Research Lab (Xu *et al*., 2003). Each mooring system was equipped with one to three AANDERAA RCM8 current meters, except for the system of Oshoro-maru, which had RCM7/8 current meters. Details of the current measurements are summarized in Table 1. The sampling interval for these current measurements was 1 hour.

Current data were first filtered with a 3-sigma quality control method to remove random uncertainty and then filtered with a 24-hour tide killer filter (Hanawa and Mitsudera, 1985), since the moored current meter data contain strong signals from near inertial oscillation (Takematsu *et al*., 1999, Mori *et al*., 2005). The power spectra of 24-hour filtered current time series show strong mesoscale variabilities, most of them ranging in a period from 10 to 100 days. Examples of the power spectra at M1 (1000 m) and M2 (2600 m) are shown in Fig. 6. Since our study concentrates on the features of mean currents, we removed eddies with periods shorter than 100 days

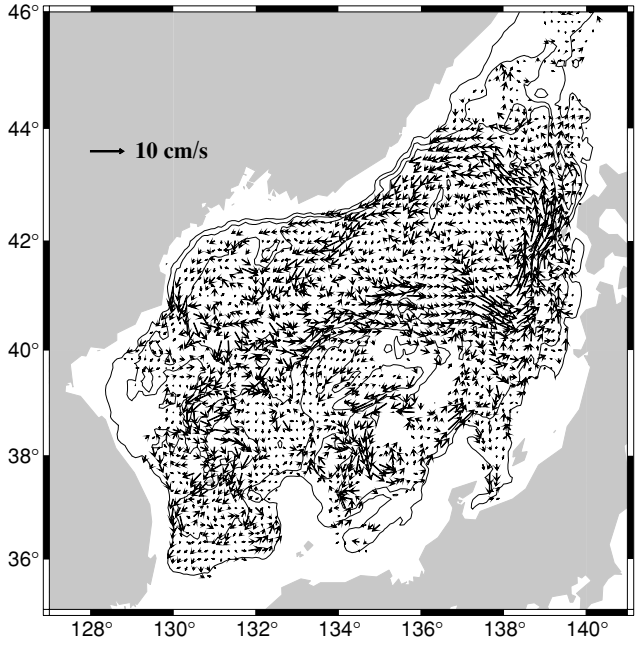

Fig. 8. Regularly gridded horizontal velocity field; the grid space is 1/6° for longitude and latitude.

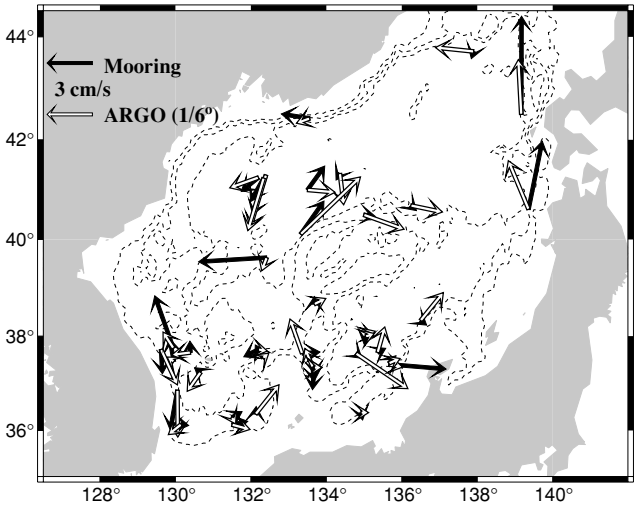

Fig. 9. Comparison between time averaged mooring current velocities at each site (black arrows) and ARGO float velocities (outlined arrows) obtained from the regularly spaced velocity field (Fig. 8). Positions of ARGO velocities indicate the nearest grid points from each mooring site.

using a low-pass filter (the Fourier Transform Band Pass Filter; FTBPF, Christiano and Fitzgerald, 2003). On the other hand, the FTBPF is applied to the time series to separate mesoscale vaiabilities with periods from 10 to 100 days.

3. Results

3.1 Annual mean deep circulation

Figure 7(a) shows the number of velocity data from float trajectories for each 1/6° × 1/6° bin. Although float observations cover a greater part of the JES, there are insufficient data in the regions east of North Korea, the YB, and north of the JB. For this reason, a large number of 1/6° × 1/6° bins do not have statistically significant numbers of velocity data, so we adopt the nearest-neighborhood routine of the Generic Mapping Tools (GMT) to average and interpolate irregularly spaced data onto regularly spaced grids (1/6° × 1/6°). An average value at a regularly spaced grid point is calculated as the weighted mean of velocity data at points located within a search radius *Rs* (25 km in this study) from the regularly spaced grid point. The weighting function is $\lambda = (1 + d^2)^{-1}$, where $d = 3r/R_s$ and r is the distance from the center of the grid. The estimated time-space mean velocities have standard errors caused by mesoscale eddies, seasonal variability, inertial oscillation, etc. For that reason, we evaluate the statistical uncertainty for the float mean velocities obtained at the parking depth. The mean velocities as well as the standard error ellipses (representing 90% confidence area) are shown in Fig. 7(b), sampled every 3 grids (1/2° interval). Each ellipse represents the area of uncertainty in the averaged velocity for each bin and the size is determined by the weighted standard deviations of u and v. More than 54% of the velocities are significant at the 90% confidence level. The most significant values are located along the cyclonic gyre in the JB.

The whole weighted-mean velocity field at the parking depth in 1/6° grid is shown in Fig. 8, which shows cyclonic circulations in the JB and YB and a complex flow pattern in the UTB. The currents in the JB and YB seem to follow steep topography deeper than 2000 m with strong velocities and are very weak in flat interiors, as noted by Hogan and Hurlburt (2000) and Senjyu *et al.* (2005). Notable features are anticyclonic eddies trapped above seamounts or rises such as the Korea Plateau north of Ulleung Island, the seamount on the Oki Spur, and two small rises on the Yamato Rise. A comparison with moored current meter data is shown in Fig. 9, revealing relatively good agreements along the periphery of each basin (e.g., HS, IS in the JB; R1 and R7 in the UTB), but poor correlation in the interior region of each basin, especially in the YB. To evaluate the correlation between current meter and ARGO float data, we adopted the vector correlation analysis proposed by Crosby *et al.* (1993), which they define as follows:

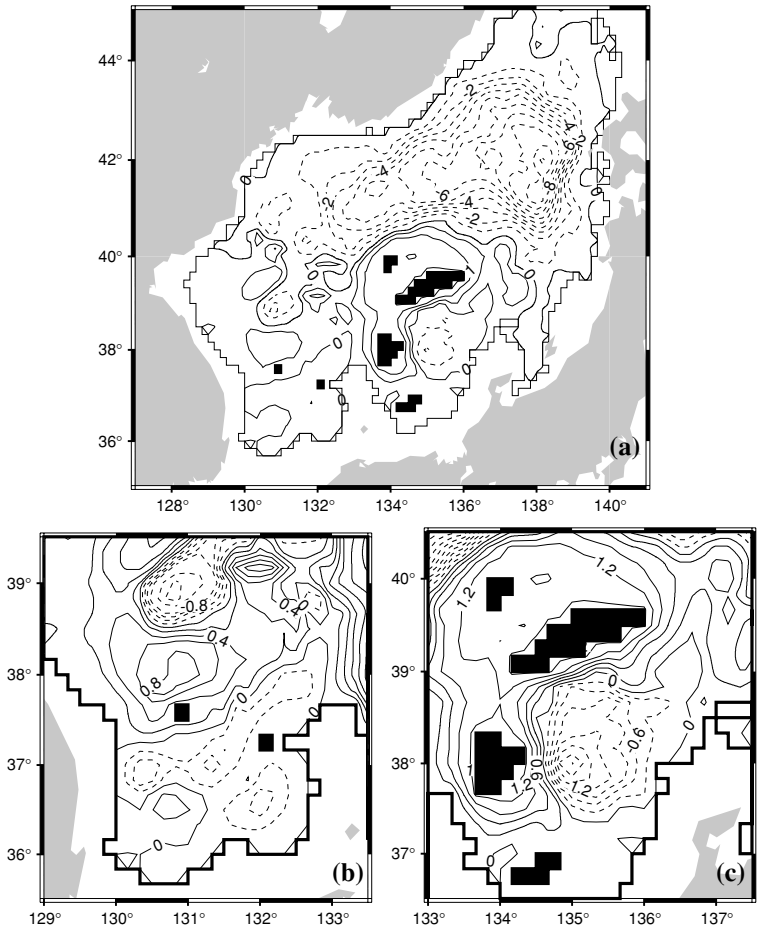

Fig. 10. Transport streamfunction from ARGO float displacements (a) for the JES deep layer (contour interval 1 Sv (<0) and 0.5 Sv (>0)), (b) for the UTB (contour interval 0.2 Sv), and (c) for the YB (contour interval 0.3 Sv), respectively.

$$\rho^2 \equiv Tr[(\Sigma_{11})^{-1}\Sigma_{12}(\Sigma_{22})^{-1}\Sigma_{21}], \quad (5)$$

where Σ_{ab} is the 2 × 2 cross-covariance matrix for the pair of vector series a and b, Tr[A] is the trace of the matrix A. The result is a scalar value which describes the similarity between two vectors. The ρ^2 is a measure of linear interdependence and ranges from 0 for no correlation to N for perfect correlation (N is dependent on the vector dimension, which is 2 in this case). In this study we use a normalized form, $\rho = \sqrt{\rho^2 / 2}$, which takes values from 0 to 1. The vector correlation between current meter and ARGO data shows a relatively high value of 0.59 for the entire region of the JES, while the northern JES (north of 40°) shows a remarkably higher correlation (0.80) than the southern part (0.42).

Next, we obtain a volume transport stream function field using the annual mean drifting velocity field in order to determine the detailed structure of volume transport in the deep layer of the JES. Since the deep velocity in the JES is considered almost uniform vertically (Takematsu *et al*., 1999), and there are no deeper Lagrangian observation data for the velocity fields, the velocity below 800 m depth is uniformly replaced by the velocity estimated from PALACE and APEX floats for the calculation of the volume transport in the deep layer from 800 m to the bottom. Senjyu *et al*. (2005) investigated the vertical variability of deep currents by progressive vector analysis using 13 current meter observations from six observation sites. We evaluated the vertical variability of mean velocities using table 1 of Senjyu *et al*. (2005). The averaged vertical shear (dU/dz) per 1000 m is only –0.01 cm/s/(1000 m), which accounts for 1.1% of mean velocity (0.91 cm/s) at six sites. The numerical data-assimilation model results provided by Hirose *et al*. (2007) also support the very small vertical differences of horizontally averaged velocities between 800 m and 3000 m (within 0.3 cm/s).

The Helmholtz theorem allows us to partition a drift-

ing velocity $\vec{u}(u, v)$ into nondivergent and irrotational components as:

$$h\vec{u} = \vec{k} \times \nabla\psi + \nabla\phi, \quad (6)$$

where $\vec{k}$ is the vertical unit vector, ψ is the streamfunction, ϕ the velocity potential, and h the thickness from 800 m to the bottom. The curl operation of Eq. (6) yields a Poisson equation as

$$\nabla^2\psi = (hv)_x - (hu)_y. \quad (7)$$

It is assumed that the regions shallower than 800 m are considered as land (islands) when solving Eq. (7). Since the calculation domain is bounded by a closed outer boundary and several islands under this assumption, the numerical solution ψ for the Poisson equation (7) is obtained using the hole relaxation method (Takano, 1974).

The volume transport streamfunction of the deep mean circulation is shown in Fig. 10. As Fig. 10(a) shows, the deep mean current follows isobaths forming a large cyclonic circulation in the JB and the volume transport of the circulation dominates mostly in regions deeper than 3000 m in the JB. A salient feature is that a strong recirculating cyclonic circulation with a zonal length scale of about 200 km is located at the deepest part of the eastern JB, as pointed out by Danchenkov *et al*. (2003). This recirculating gyre is accompanied by very strong northward currents reaching 4~6 cm/s on its eastern rim, which were also observed by moored current meters at sites IS and HS in Fig. 9 (Senjyu *et al*., 2005). It should be noted that the maximum volume transport of the large cyclonic gyre in the JB reaches about 10 Sv (1 Sverdrup = 10^6 m^3s^{-1}), which is about four times greater than that of the Tsushima Warm Current through the Tsushima Straits. The flow pattern corresponds well to trajectories of nine PALACE floats over the JB observed in 1999 to 2001 by Danchenkov *et al*. (2003).

The deep circulation in the southwestern deep JES in Fig. 10(b) shows a more complicated flow pattern than that in the JB, partly due to the complicated bottom topography in this region. The southward deep currents following the isobaths shallower than 3000 m along the western periphery of the JB flow into the southwestern deep JES. They finally enter the UTB, accompanied by a cyclonic eddy in a small basin with a center at (39°N, 131°E) north of the Korea Plateau and two anticyclonic eddies with centers at (39.2°N, 132.0°E) and (38.2°N, 131°E). The former might be generated by mesoscale eddy effects with a time scale longer than 1 year and the latter anticyclonic eddy is trapped by the Korea Plateau.

The circulation pattern in the UTB is generally weak and cyclonic, accompanied by sub-basin scale cyclonic and anticyclonic eddies, as noted by Teague *et al*. (2005). The current entering the UTB from the JB through the Ulleung Interplain Gap† (UIG) continues to flow southwestward until it bifurcates into two branches, a northward and southward branch near the Korean coast around (37.5°N, 130.3°E). The northward branch along the southwestern periphery of the anticyclonic eddy over the Korea Plateau corresponds well to the northward deep current over the Korea Plateau by Teague *et al*. (2005), who suggested an anticyclonic circulation pattern over the Korea Plateau. The southward branch circulates the UTB cyclonically, alternately accompanied by a cyclonic, anticyclonic, and cyclonic eddies.

It should be noted that the floats captured the southward boundary currents from 38°N to 36°N along the Korean coast, as seen in Fig. 8. These southward currents were reported by Chang *et al*. (2002) and Teague *et al*. (2005), and are considered to be a continuation of the North Korean Cold Current, as suggested by Park *et al*. (2004).

The inflow and outflow transports through the UIG for the deep layer are 0.7 and 0.3 Sv, respectively, yielding a net transport of 0.4 Sv into the basin. On the other hand, Teague *et al*. (2005) calculated the volume transport from 250 m to the bottom through the UIG using NLOM (Navy Layered Ocean Model) results, obtaining 0.68 Sv and 0.38 Sv as the inflow and outflow transports, respectively, and yielding a net transport of 0.3 Sv into the basin, which is smaller than our estimate.

The mean circulation appearing in the YB in Fig. 10(c) is characterized by a relatively strong cyclonic circulation with a volume transport of 2 Sv and a small anticyclonic eddy over the Oki Spur west of the YB, which is also seen in Fig. 8. Strong southwestward currents in Fig. 8, which are northern rim currents of the cyclonic circulation in the YB, reach about 7~8 cm/s, showing good agreement with the moored current meter data published by Senjyu *et al*. (2005). The northwestward current (2~3 cm/s) through the southern gap (around 37.5°N) of the Oki Spur in Fig. 8 was also observed by moored current observations (Senjyu *et al*., 2005), while the relatively small eastward current through the northern gap (around 38.5°N) of the Oki Spur in Fig. 8 was not observed by Senjyu *et al*. (2005). Although the mean flow pattern in Fig. 10(c) reflects some observed features, it should be noted that the drifting current data density in the YB is not dense enough to discuss details of mean flow pattern in the YB as inferred from the confidence level in the YB in Fig. 7(b).

It is generally believed that deep mean currents primarily follow ambient potential vorticity contours (f/H), where f is the Coriolis parameter and H is the depth. However, as seen in the circulation in the UTB, the extent to

†The "Ulleung Interplain Gap" corresponds to the "Oki Gap".

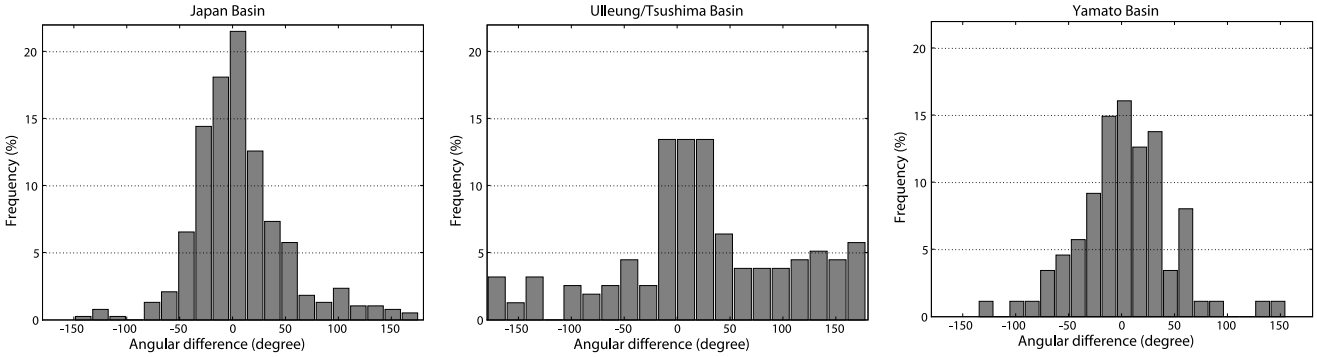

Fig. 11. Histograms of angular differences between the *f*/*H* direction and non-divergence velocity field in the deep layer (800 m to bottom) at the JB (left), UTB (center), and YB (right), respectively. Correlation coefficients of each region are 0.82, 0.40, and 0.77, respectively. ¶The Editor-in-Chief does not recommend the usage of the term "Ulleung Basin" in place of "Tsushima Basin".

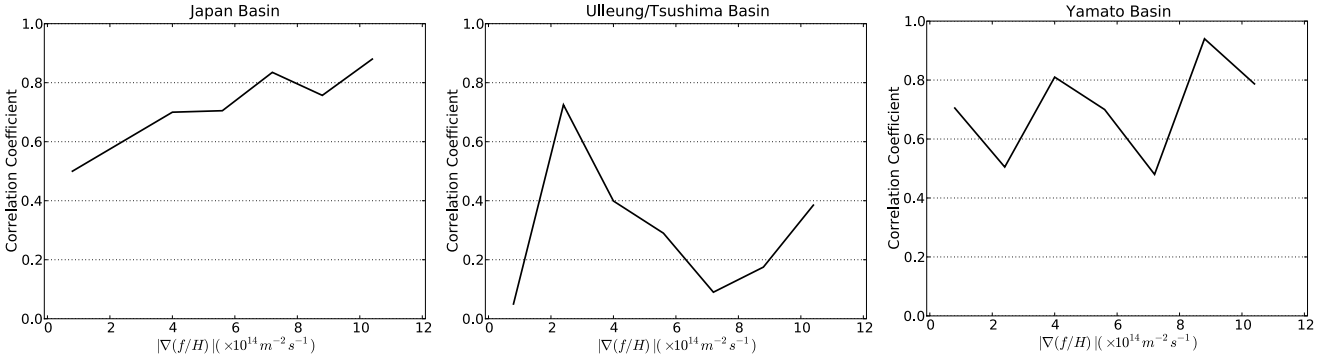

Fig. 12. Correlation coefficients between directions of streamlines and directions of *f*/*H* contours in the JB (left), UTB (center), and YB (right), respectively. Correlation coefficient for each graph is calculated with the grids where $|\nabla(f/H)|$ is between each interval of 1.5×10^{14} $m^{-2}s^{-1}$. ¶The Editor-in-Chief does not recommend the usage of the term "Ulleung Basin" in place of "Tsushima Basin".

which the deep mean current follows *f*/*H* depends on the situation in each basin. To check how ambient potential vorticity constrains the flow pattern of deep mean flow, the contours of volume transport stream function in Fig. 10(a) are compared with the contours of *f*/*H*.

In the comparison of ambient potential vorticity and stream function, we calculated a pair of (u, v) fields from stream function and *f*/*H* values, respectively. Because our interest is in contour direction but not in non-divergent velocity speed or magnitude of *f*/*H* vector, we normalized the velocity amplitude and magnitude of *f*/*H*.

Figure 11 shows the distribution of angle differences of directions between streamlines and *f*/*H* contours. The histograms of angle differences show roughly Gaussian distributions in the JB and YB. In the UTB the histogram is widely distributed with a correlation coefficient (0.40), which is much less than those in other regions (r = 0.82 and 0.77 in the JB and YB, respectively). Hogan and Hurlburt (2000) noted that abyssal variabilities of pressure and eddy kinetic energy are non-deterministic over areas with relatively flat topography, and deep flows instead tend to follow PV (potential vorticity) contours when $|\nabla(f/H)|$ is large. The dependence of the correlation coefficient between directions of streamline and *f*/*H* contours on the $|\nabla(f/H)|$ is shown in Fig. 12. The correlation coefficients show a tendency to increase as $|\nabla(f/H)|$ becomes large in the JB and YB and reach remarkably high values (>0.8) in a steep slope region where $|\nabla(f/H)|$ is larger than 9×10^{14} $m^{-2}s^{-1}$ in both the JB and YB, suggesting that deep flow tends to follow PV contours when $|\nabla(f/H)|$ is large, as suggested by Hogan and Hurlburt (2000). On the other hand, the correlation coefficient in the UTB shows a different tendency, which has maximum correlation when $|\nabla(f/H)|$ is small (about 2×10^{14} $m^{-2}s^{-1}$), with intense fluctuation. However, due to the low density of data, as seen in Fig. 7(a), and the resulting poor confi-

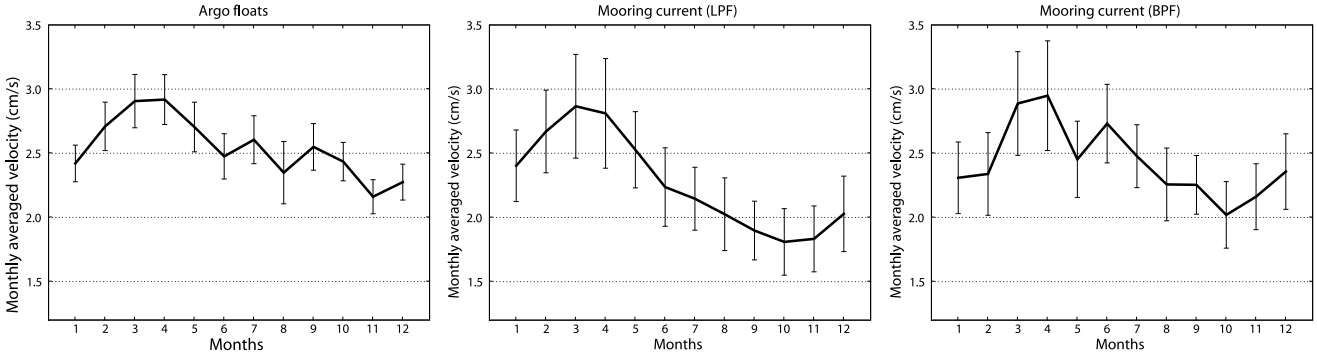

Fig. 13. Monthly averaged deep current velocities from 4632 ARGO float displacements (left), 100-day low-pass-filtered 78 mooring time series (LPF, center), and 10 to 100 days band-pass-filtered 78 mooring time series (BPF, right), respectively. Vertical bars indicate standard errors for each month with 90% confidence interval.

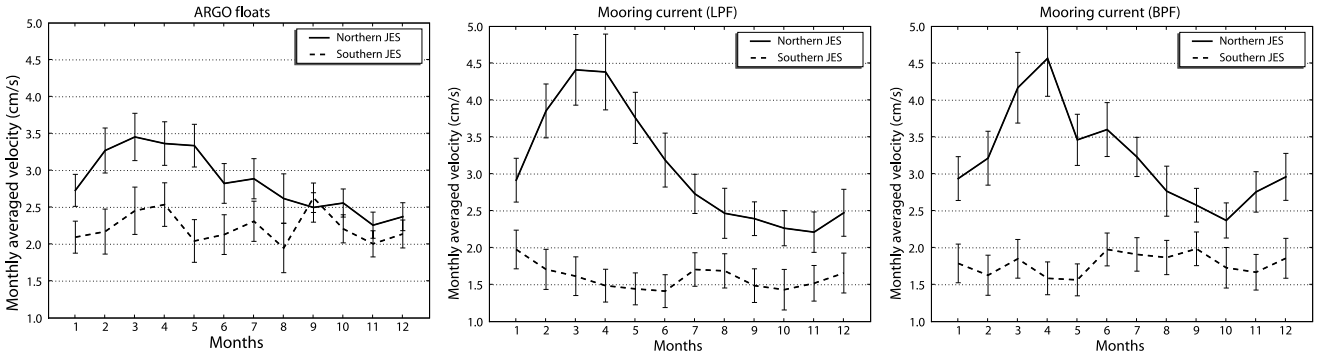

Fig. 14. As Fig. 13 except that solid lines represent the northern JES (north of 40°N), whereas dashed lines represent the southern JES (south of 40°N).

dence of the mean velocity in the YB, as seen in Fig. 7(b), it would be difficult to conclude at this stage that deep flow in the YB tends to follow PV contours when $|\nabla(f/H)|$ is large.

3.2 Seasonal variations of current velocities

The seasonal changes of monthly averaged velocity amplitudes calculated from profiling floats (left), 100-day low-pass-filtered mooring current meter data (LPF, center), and 10 to 100 days band-pass-filtered mooring current meter data (BPF, right) are shown in Fig. 13, where each monthly mean includes standard errors of observed velocities for each month plotted as a vertical bar (at 90% confidence level). A salient feature in both profiling float and current meter data is that the monthly mean velocity increases from late fall to reach a maximum in early spring, then decreases gradually toward fall until the start of the strong northwest monsoon.

The mean velocities from profiling floats show remarkable seasonal variations with a maximum of 2.9 cm/s in April, a minimum of 2.2 cm/s in November. Similar patterns are observed in the current meter data: the maximum and minimum of LPF (BPF) are 2.8 cm/s (2.9 cm/s) in March (April) and 1.8 cm/s (2.0 cm/s) in October (October), although the phase of each graph is slightly different. Corresponding annual averages of profiling floats, LPF and BPF, are 2.6 cm/s, 2.2 cm/s and 2.4 cm/s, respectively.

These seasonal changes were also reported by Takematsu *et al*. (1999). However, since they did not separate currents into mean current and eddy activity in the study of seasonal change, it was not clear whether the mean deep current showed such seasonal variations. These seasonal variations of deep mean current were successfully reproduced numerically by Luneva and Clayson (2006), who reported that the seasonal variation of deep mean current follows f/H contours with a maximum in March and two minima during August to November, using a sigma-z version of the CUPOM (Colorado University Princeton Ocean Model) with 6-km resolution and 38 vertical levels. Figure 14 shows seasonal variations of the deep mean currents separately in the northern (north

of 40°N, solid lines) and southern part (south of 40°N, dashed lines) of the JES. Left, center and right panels in Fig. 14 correspond to profiling floats, LPF and BPF, respectively, showing that the seasonal variation with a maximum in early spring and minimum in fall is dominant in the northern JES in both profiling float and moored current meter data (LPF and BPF), whereas the data from the southern JES do not show any notable seasonality.

It should be noted that in the northern JES the maximum velocity for the moored current meter data is about 1.3 times greater than the monthly average of profiling floats. The lack of wide coverage of the current meter mooring system may be one of the reasons for this difference in the amplitude of deep mean currents.

4. Summary and Discussion

The horizontal structure of deep mean circulation and its seasonal variability in the JES were studied using profiling floats and moored current meter data. The deep mean currents in the JB flow cyclonically, generally following ambient potential vorticity (f/H) contours, which is in agreement with previous studies (Hogan and Hurlburt, 2000; Senjyu *et al*., 2005). The correlations between directions of deep current and f/H contours increase as $|\nabla(f/H)|$ increase, with remarkably high values of correlation coefficient (>0.8) in steep slope regions in the JB. However, due to the low density of data in the YB, it would difficult to conclude that the correlation between deep mean currents and f/H contours in the YB has the same tendency as that in the JB.

It is notable that the time-space averaged deep mean current in the JB is about 2.8 cm/s and its volume transport in the deep layer (800 m to bottom) reaches about 10 Sv, which is about four times larger than the inflow transport through the Tsushima Straits.

On the other hand, the UTB shows a lower correlation between directions of deep current and f/H contours than other basins. Unlike the deep mean circulations in the JB, the circulation in the UTB is generally weak and cyclonic, accompanied by sub-basin scale cyclonic and anticyclonic eddies, as noted by Teague *et al*. (2005). These results in the UTB suggest that not only eddy-topography interaction but also other dynamic links between the surface and deep layer are at work in the formation of deep mean currents in the UTB. The inflow and outflow transports through the UIG for the deep layer are 0.7 and 0.3 Sv, respectively, yielding a net transport of 0.4 Sv into the basin. More observational and modeling efforts should be undertaken to clarify the mechanism of the deep circulation system in the UTB.

Analysis of profiling float data shows that the deep mean current in the northern JES, substantially the JB, is accompanied by a remarkable seasonal variation with a maximum in March and minimum in November. The annual range of the seasonal variation is about 30% of the mean velocity. The same tendency of the seasonal variation can be seen in the current meter data, although the amplitude in spring is slightly stronger than that found in the profiling float data. Reflecting the seasonal variability of deep currents, the volume transport can be expected to show a similar seasonal variation with a maximum in March and minimum in fall with an annual range of 3 Sv (30% of the average volume transport of 10 Sv). It should be noted that the deep mean currents in the southern JES (YB and UTB) in both profiling float data and moored current meter data (LPF and BPF) are weak and do not show such a notable seasonal variability as in the northern JES. The reason for the difference in the deep mean current seasonal change between the northern and southern JES is a open question.

One mechanism to generate the seasonal variation of deep mean current is surface forcing, that is, wind stress and thermohaline forcing, which have a similar seasonal variation to that of the deep mean current in the northern JES. However, the wind stress itself and thermohaline forcing may not be able directly to induce a strong mean current greater than a few cm/s in the deep layer, as seen in the outcomes of many numerical models without sufficient resolution to resolve mesoscale eddies, e.g., Kim and Yoon (1996). The other candidate is baroclinic eddies generated through baroclinic instability at the surface. Energy transfer by baroclinc eddies at the surface to the deep layer has been studied by many authors (Dewar, 1998; Greatbatch, 1998; Greatbatch and Li, 2000; Hogan and Hurlburt, 2000). Hogan and Hurlburt (2000) showed the transfer of baroclinic eddy energy at the surface to the deep ocean, successfully reproducing the eddy-driven deep mean flow following the f/H contour in the Japan Sea using a primitive four layer model with extra-fine horizontal resolution (<1/32°). The Hogan and Hurlburt (2000) results suggest that the deep mean current in the JB in Fig. 14 is possibly generated through eddy-mean flow interaction. But the reason for the significant seasonal variation in the northern JES, as seen in Fig. 14, is still an open question, as is the reason for the weakness and aseasonality of the deep mean current in the southern JES. More data analysis and numerical model studies are required to clarify the mechanism of the seasonal variation.

Acknowledgements

We especially thank Professor Riser for allowing us to use his PALACE observation data. KMA provided their APEX float trajectory data. We would also like to thank the officers and crew of the T/S Kakuyo-maru, R/V Professor Khromov, and T/S Oshoro-maru for their dedication during the observation campaign. The current meter data were provided by Dr. Teague of Rhode Island Uni-

versity, supported by the United States Office of Naval Research "Japan/East DRI".

References

Chang, K. I., N. G. Hogg, M.-S. Suk, S.-K. Byun, Y.-G. Kim and K. Kim (2002): Mean flow and variability in the southwestern East Sea. *Deep-Sea Res., Part I*, **49**, 2261–2279.

Christiano, L. J. and T. J. Fitzgerald (2003): The Band Pass Filter. *Internat. Economic Rev.*, **44**(2), 435–465.

Crosby, D. S., L. C. Breaker and W. H. Gemmill (1993): A proposed definition for vector correlation in geophysics: theory and application. *J. Atmos. Oceanic Technol.*, **10**, 355–367.

Danchenkov, M. A., S. C. Riser and J.-H. Yoon (2003): Deep currents of the central Sea of Japan. *Pacific Oceanogr.*, **1**, 6–11.

Davis, R. E., D. C. Webb, L. A. Regier and J. Dufour (1992): The Autonomous Lagrangian Circulation Explorer (ALACE). *J. Atmos. Oceanic Technol.*, **9**, 264–285.

Dewar, W. K. (1998): Topography and barotropic transport control by bottom friction. *J. Mar. Res.*, **56**, 295–328.

Greatbatch, R. J. (1998): Exploring the relationship between eddy-induced transport velocity, vertical momentum transfer and the isopycnal flux of potential vorticity. *J. Phys. Oceanogr.*, **28**, 422–432.

Greatbatch, R. J. and G. Li (2000): Alongslope mean flow and an associated upslope bolus flux of tracer in a parameterization of mesoscale turbulence. *Deep-Sea Res., Part I*, **47**, 709–735.

Hanawa, K. and M. Mitsudera (1985): About constructing of daily mean values of ocean data. *Coastal Research Note*, **23**, 79–87.

Hirose, N., H. Kawamura, H. J. Lee and J.-H. Yoon (2007): Sequential forecasting of the surface and subsurface conditions in the Japan Sea. *J. Oceanogr.*, **63**, 467–481.

Hogan, P. J. and H. E. Hurlburt (2000): Impact of upper ocean topographical coupling and isopycnal outcropping in Japan/East Sea simulations with 1/8° to 1/64° resolution. *J. Phys. Oceanogr.*, **30**, 2535–2561.

Ichikawa, Y., Y. Takatsuki, K. Mizuno, N. Shikama and K. Takeuchi (2001): Estimation of drifting velocity and error at parking depth for the ARGO float. Technical report, Argo Technical Report, FY2001.

Kim, C.-H. and J.-H. Yoon (1996): Modeling of the wind-driven circulation in the Japan Sea using a reduced gravity model. *J. Oceanogr.*, **52**, 359–373.

Kitani, K. (1987): Direct measurement of the Japan Sea Proper Water. *Report of Japan Sea National Fish. Res. Inst.*, **341**, 1–6 (in Japanese).

Luneva, M. V. and C. A. Clayson (2006): On the formation of abyssal currents in the Japan (East) Sea. *EOS Trans. AGU, Ocean Sci. Meeting Suppl.*, **87**(36), abstract OS16J-18.

Mori, L., T. Matsuno and T. Senjyu (2005): Seasonal/spatial variations of the near-inertial oscillations in the deep water of the Japan Sea. *J. Oceanogr.*, **61**, 761–773.

Park, Y. G., K. H. Oh, K.-I. Chang and M.-S. Suk (2004): Intermediate level circulation of the southwestern part of the East/Japan Sea estimated from autonomous isobaric profiling floats. *Geophys. Res. Lett.*, **31**, L13213.

Sallée, J.-B., N. Wienders, K. Speer and R. Morrow (2006): Formation of subantarctic mode water in the southeastern Indian Ocean. *Ocean Dynamics*, **56**, 525–542.

Senjyu, T., H.-R. Shin, J.-H. Yoon, Z. Nagano, H.-S. An, S.-K. Byun and C.-K. Lee (2005): Deep flow field in the Japan/East Sea as deduced from direct current measurements. *Deep-Sea Res., Part II*, **52**, 1726–1741.

Takano, K. (1974): A general circulation model for the world ocean. Numerical Simulation of Weather and Climate. Tech. Rep. No. 8, Department of Meteorology, Univ. of California, Los Angeles, 47 pp.

Takematsu, M., Z. Nagano, A. Ostrovskii, K. Kim and Y. Volkov (1999): Direct measurements of deep currents in the northern Japan Sea. *J. Oceanogr.*, **55**, 207–216.

Teague, W. J., K. L. Tracey, D. R. Watts, J. W. Book, K.-I. Chang, P. J. Hogan, D. A. Mitchell, M.-S. Suk, M. Wimbush and J.-H. Yoon (2005): Observed deep circulation in the Ulleung Basin. *Deep-Sea Res., Part II*, **52**, 1802–1826.

Tomczak, M. (2007): Variability of Antarctic intermediate water properties in the South Pacific Ocean. *Ocean Sci.*, **3**, 363–377.

Xie, J., J. Zhu, L. Xu and P. Guo (2005): Evaluation of mid-depth currents of NCEP reanalysis data in the tropical Pacific using ARGO float position information. *Adv. in Atmos. Sci.*, **22**, 677–684.

Xu, Y., K. L. Tracey, D. R. Watts, M. Wimbush and W. Teague (2003): Current Meter Data Report: Ulleung Basin in the Japan/East Sea. University of Rhode Island, Graduate School of Oceanography Technical Report, August 2003, 119 pp.

Yanagimoto, D. and K. Taira (2003): Current measurements of the Japan Sea Proper Water and the Intermediate Water by ALACE floats. *J. Oceanogr.*, **59**, 359–368.